Research Square

Preprints are preliminary reports that have not undergone peer review.
They should not be considered conclusive, used to inform clinical practice,
or referenced by the media as validated information.

Head-dynamic admissibility: physically constrained separation of estimated head motion and sensor-relative motion in wearable inertial recordings

Jyrki Launes

jyrki.launes@helsinki.fi

University of Helsinki https://orcid.org/0000-0002-3477-398X

Kati Peltonen

University of Helsinki

Matti Vartiainen

University of Helsinki

Tommi Makkonen

University of Helsinki

Jaakko Kauramäki

University of Helsinki

Laura Hokkanen

University of Helsinki

Research Article

Keywords: head motion, wearable inertial sensor, sensor coupling, angular velocity, head impact, signal decomposition, football heading, women's ice hockey, mechanical exposure

Posted Date: November 19th, 2026

DOI: https://doi.org/10.21203/rs.3.rs-11759335/v1

License: This work is licensed under a Creative Commons Attribution 4.0 International License.
Read Full License

Additional Declarations: The authors declare potential competing interests as follows: J.L. is named as an inventor on a pending patent application filed with the Finnish Patent and Registration Office concerning methods for extracting and representing waveform-derived features from wearable head-impact sensor data, including aspects of the Impact Feature Space methodology used in this

manuscript. The patent application was filed before submission of the manuscript. No licensing income or commercial revenue has been received. The other authors declare no competing interests.

Abstract

Background.

A wearable inertial sensor measures the movement of its own housing. Even when the device sits firmly against the mastoid, a recorded head-impact waveform can contain movement of the sensor with respect to the skull. Low-pass filtering and whole-record rejection suppress unwanted structure, but neither estimates which part of a measured angular-velocity trajectory is compatible with movement of the head.

Methods.

We developed head-dynamic admissibility (HDA), a constrained decomposition of triaxial gyroscope signals into an estimated head angular velocity and a bounded sensor-relative component. The model limits sensor-relative angular excursion and minimises post-contact inertial demand, and it accounts for gyroscope quantisation and saturation. We tested recovery on synthetic trajectories carrying known injected relative movement, then applied HDA version 0.1.2 to 341 video-classified football events (233 headers and 108 non-headers) and to 17,607 gyroscope-analyzable recordings from two women's elite ice-hockey teams during the 2025–2026 season. We calculated frozen Impact Feature Space (IFS) descriptors and H1 scores from the recorded signal and from the HDA head estimate.

Results.

Synthetic injection tests separated injected sensor-relative ringing from smooth-head nulls with an area under the receiver operating characteristic curve of 0.94 to 1.00 across the tested configurations; waveform correlations were 0.83 to 0.91 and head-trajectory error fell by 43 to 58%. In both field datasets the size of the correction depended on the class of descriptor. Integral angular activity changed little in the video-classified football recordings (median 2.57% in headers and 2.26% in non-headers), whereas C01, C03, C06 and C07 changed substantially. The same pattern held across the 17,607 hockey recordings, where median changes were 1.69% for C05 and 4.51% for C02 against 25.91% for C01, 25.90% for C03 and 21.13% for C07. Overall H1 changed by a median of − 2.73 points.

Conclusions.

From a single mastoid-mounted gyroscope, HDA yields an explicitly constrained estimate of head angular motion together with the sensor-relative component that accompanies it. Because the size of that correction varies systematically across waveform descriptors, sensor coupling can be assessed directly when single events are interpreted and when longitudinal mechanical-exposure summaries are

built. The field recordings carry no independent skull kinematics against which the estimate could be checked.

1 Introduction

Wearable inertial sensors are widely used to quantify head acceleration events in sport [1, 2]. Whatever the mounting, skin patch, headband, helmet or mouthguard, such a device measures the kinematics of its own housing and not those of the skull. Two mechanically distinct contributions therefore occur together in the measured waveform: motion imposed on the sensor by the moving head, and motion of the sensor with respect to the head that arises from the compliance, inertia and contact conditions of the attachment. We term these *head motion* and *sensor-relative motion*. Separating them matters whenever the quantity of interest is movement of the head and not movement of the instrument.

The second contribution can be substantial. In vivo comparisons of skull-coupled and less rigidly coupled sensors show displacement with respect to the skull, overestimated kinematics and damped oscillatory sensor signals [3]. Laboratory impact tests document relative motion between helmet and head [4, 5], and compromised coupling of an instrumented mouthguard can produce oscillatory high-frequency content and spurious angular-acceleration peaks in field recordings [6–8, 27]. The mechanical interface differs across these devices, but together the findings establish that coupling matters. Bandwidth and sampling rate shape the recorded waveform as well [9], and consensus procedures for wearable head-kinematic devices address coupling explicitly in both laboratory and on-field evaluation [10, 11].

Common processing remains largely sensor-centric. The recorded waveform is first treated as head motion, and components believed to be noise or artefact are then suppressed by low-pass filtering, spectral screening or rule-based rejection [7, 12]. Such steps can improve consistency, yet they leave open which components represent head kinematics, and the frequency ranges of head movement and of compliant attachment movement may overlap. The Impact Feature Space (IFS) describes a recording through temporally and directionally resolved mechanical descriptors instead of peak values alone [13]. In an exploratory IFS filtering experiment, integrated angular descriptors were comparatively resistant to low-pass filtering, while acceleration-dependent and directional-path descriptors were more sensitive. Filtering locates fast structure; on its own it does not assign that structure to the head or to the mounting.

The distinction that matters is mechanical. An adult head has a mass of about 4–5 kg, documented moments of inertia [14] and dynamical coupling to the neck and trunk [15, 16]. Outside the brief interval of externally forced contact, head movement must stay compatible with the passive and active neck torques available [17, 18]. The mastoid-mounted ACT sensor weighs a few grams and is held against the skin by an elastic headband. It follows head movement broadly while it may undergo small additional translations or rotations with respect to the skull. An excursion of less than a degree can generate a

considerable short-duration angular-velocity or angular-acceleration signal without implying rotation of the head at the same rate.

From measured quantities alone, a single six-axis sensor cannot separate the two contributions uniquely. The full rigid-body measurement model leaves head translation, head rotation, relative sensor orientation and relative sensor position all unknown, so any decomposition depends on physically motivated restrictions. We make no claim to observe skull angular velocity directly through an independent reference device. Head-dynamic admissibility (HDA) asks a narrower question: can a gyroscope trajectory be represented as plausible head movement plus a sensor-relative angular excursion confined to an explicit envelope? The decomposition measures how much of the post-contact head-side inertial demand can be reassigned to such a bounded excursion while the observed measurement is still reproduced.

Our principal aim was to formulate this head-motion estimator, build it in software and examine how it behaves. Synthetic waveforms with known injected relative motion establish that behaviour under controlled assumptions. The main empirical demonstration uses football headings, for which individual events carry independently video-reviewed labels. A second demonstration draws on an extended women's ice-hockey dataset, where we ask how the correction changes mechanical descriptors across many repeated recordings and what quantitative basis it gives for assessing cumulative exposure. We left the published IFS representation unchanged and recomputed its descriptors separately on recorded angular velocity and on the HDA-estimated head angular velocity [13]. Kinematic features can be used to classify triggered events [23], but classification here is secondary to the quality and mechanical interpretation of the estimated movement.

2 Methods

2.1 Study design and sensor

We report a methodological development and a secondary analysis of existing sports-sensor recordings. The data come from the ACT Head Impact Tracker Pro (Northern Sports Insight and Intelligence Oy, Finland), a six-axis inertial sensor of about 5 g held against the skin over the mastoid region by a fitted elastic headband. Each triggered record holds 76 samples at 1 kHz of three-axis linear acceleration and three-axis angular velocity. Recorded linear acceleration drives the trigger, and the configured threshold varies by recording protocol (5 g or 10 g). Within HDA, linear acceleration marks the contact interval and supplies context for the quality indicators; it is not used to estimate translational head motion. Gravity is not modelled.

Gyroscope resolution is 1°/s (0.017453 rad/s) and saturation 2000°/s per axis (34.9066 rad/s). Because the gyroscope starts later than the accelerometer, the algorithm locates the first usable gyroscope sample and omits the non-measurement samples that precede it. In the available flattened files these cluster strongly at sample 8, and the files carry a documented earlier extractor convention that blanked

the first eight gyroscope samples. Nothing can recover those early samples after the fact. HDA flags saturated samples and drops them from the corresponding inertial-demand rows while keeping the events for descriptive reporting; it does not reconstruct saturated measurements.

2.2 Football: video-verified individual events

Two adult football-tennis heading practice sessions took place on 13 July 2026 (male athletes) and 20 July 2026 (female athletes). Their HDA v0.1.2 exports hold 346 and 413 triggered records. Of these, 299 and 330 were initial triggers and 47 and 83 were retriggers. The independently corrected video-review master identifies 341 unique eligible initial-trigger recordings: 233 headers (117 male and 116 female) and 108 non-headers (77 male and 31 female). One reviewer assigned the labels from synchronised two-camera video. Handling, unclear and unreviewed events did not enter the header-versus-non-header classification. We verified the match to the HDA outputs one-to-one on sex, sensor profile, event index and timestamp. Repeated-trigger sequences followed the existing protocol, and the first record of each was retained for the video-classification sample.

The primary football outcome is the paired change in estimated rotational waveform descriptors for individual video-confirmed events. We report headers and non-headers separately, since neither group can be assumed mechanically homogeneous. Differences between the male and female training sessions fall outside the scope of this article, because session and sex are confounded with technique, acquisition and fitting conditions. Sex-related effects enter only where they are needed to interpret the HDA results.

2.3 Ice hockey: season-wide sensor recordings

We applied HDA v0.1.2 to recordings from two teams in Finland's top women's ice-hockey league, Auroraliiga, during the 2025–2026 season. The source comprises 10,216 HIFK and 8,817 K-Espoo trigger records, 19,033 in total. Gyroscope signals were available and HDA solutions obtained for 8,852 and 8,755 events, giving 17,607 events in the primary whole-cohort mechanical-descriptor analysis. These recordings overlap the smaller 4,402-event cohort of the accepted IFS methods paper [13] and do not form an independent replication dataset.

The season was classified separately with Wisehockey player tracking and match timing [19]; on-ice activity is a determination of event context and not proof of head contact. Off-ice recordings remain in the full-cohort methodological analysis. The cumulative-exposure analysis set out in Supplementary Section D.6 is restricted to events already classified as on-ice participation, and it awaits the linkage of that classification and of the Wisehockey time-on-ice denominators, neither of which is embedded in the supplied HDA v0.1.2 export files.

2.4 Kinematic measurement model

Let ω_H denote head angular velocity, R the orientation of the sensor relative to the head, $\omega_{S/H}$ the relative angular velocity of the sensor, and e_ω gyroscope transduction error. The measured sensor-frame angular velocity is

$\omega_S(t) = R(t)^{\top} \omega_H(t) + \omega_{S/H}(t) + e_{\omega}(t)$. (1)

With the accelerometer measuring specific force, the corresponding translational measurement depends further on head reference-point acceleration, rotational acceleration, the offset to the sensor and its relative displacement, through tangential, centripetal and relative-motion terms (Supplementary Section A). Six measurements cannot determine the full set of head and relative states, so the complete model is not identifiable without additional assumptions. HDA applies a small-angle approximation to the sensor-relative orientation and confines estimation to the angular channels.

2.5 Sensor-relative excursion and head-side inertial demand

We assume that the sensor-relative orientation e stays within a finite angular envelope of radius θ_{max} during a record. For a sinusoidal relative rotation of amplitude θ and frequency f, angular velocity and angular acceleration have amplitudes $\theta(2\pi f)$ and $\theta(2\pi f)^2$. A small relative excursion can thus produce a substantial derivative signal. In the implementation, sensor-relative angular velocity is the first discrete difference of e divided by the sampling interval, and the free centre of the excursion envelope is not identifiable. The bound applies to the full relative angular-state vector and is not an arbitrary frequency cutoff.

Outside the accelerometer-defined contact interval, the estimated head trajectory is penalized by a squared inertial-torque demand,

$J(\omega_H) = \Delta t \sum_{k \notin C} \sum_{j \in \{a,b,c\}} [\, I_j (\omega_{H,j}[k+1] - \omega_{H,j}[k]) / \Delta t \,]^2$, (2)

where $\Delta t = 0.001$ s, C is the contact interval and the assigned principal moments of inertia are (0.0230, 0.0243, 0.0158) kg·m² [14]. Only stencil rows lying outside contact and free of saturation contribute to the demand. The functional expresses inertial smoothness and does not amount to a calibrated head-neck constitutive model. The contact interval opens at the first contiguous run of resultant linear acceleration at or above 5 g and closes 2 ms after that run ends. This 5 g value is the HDA contact-definition parameter and need not equal the acquisition trigger threshold.

A quantisation dead-band allows an axis-specific measurement perturbation n with $|n_j| \le q/2$, where q = 1°/s. For measured gyroscope samples $m = g_0, \ldots, 75$, the small-angle discrete decomposition is

$\omega_S[m] = \omega_H[m] + (e[m+1] - e[m])/\Delta t + n[m]$. (3)

The rigid-coupling reference minimises J under the dead-band alone, yielding J_q. The bounded-excursion hypothesis minimises the same demand while allowing $\|e[k]\|_2 \le \theta_{max}$ at each state node, yielding $J_1(\theta_{max})$. Their relative difference,

$\Delta J_{rel}(\theta_{max}) = \{J_q - J_1(\theta_{max})\} / J_q$, (4)

measures the proportion of rigid-coupling head-side demand that can be removed by a sensor-relative excursion satisfying the specified bound. Both hypotheses reproduce the observed measurement under different constraints, which makes ΔJ_rel a constrained attribution statistic and not an observed probability of artefact.

A small quadratic tie-break penalty keeps unconstrained constant or slowly varying components from being assigned arbitrarily to sensor-relative motion; we fixed its characteristic frequency at 5 Hz. Clarabel solved the resulting constrained quadratic program [20]. We evaluated six excursion radii, 0.05°, 0.1°, 0.25°, 0.5°, 1° and 2°, and used the predefined 0.25° solution to recompute the frozen IFS descriptors. The reported head estimate subtracts the attributed sensor-relative angular velocity from the recorded gyroscope signal and leaves quantisation as measured. Supplementary Section A gives the full discretisation, the solver conventions and the verification.

2.6 HDA outputs, quality indicators and synthetic validation

HDA describes the decomposition at several levels, so that the inferred head motion can be examined beside the motion attributed to the attachment. For every recording it reports the inertial demand under rigid coupling and the relative reduction of that demand across the specified sensor-excursion limits. The output further carries the fraction of angular-velocity energy assigned to sensor-relative motion, its peak angular velocity and acceleration, the excursion the solution used, and θ_{50}, the excursion scale at which half of the maximum demand reduction is reached. Two quantities represent the temporal character of the attributed component: its effective frequency and its distribution across four phases of the recording spanning 0–12, 12–25, 25–50 and 50–76 ms. Version 0.1.2 adds information on the stability of the contact definition, gyroscope saturation, provisional reasons for mechanical inadmissibility and a rule-based artefact-point indicator. All of these describe properties of a recording under stated criteria. None is a calibrated probability that an event is an artefact, and none served as independent grounds for excluding events here, where we retained the established technical validity rules.

Synthetic recordings let us examine the decomposition under controlled conditions in which both the modelled head motion and any added sensor-relative motion were known. The original null set held 1,000 smooth rigid-head events, each combining a short acceleration-defined contact pulse with a gamma-shaped rotational pulse, a slowly varying rotation axis and a damped low-frequency head-neck component. The simulated measurement process reproduced delayed gyroscope activation, quantisation and saturation. To examine recovery of additional motion at the attachment, we injected damped sensor-relative rotations into 200 recordings for each tested configuration. Injected excursion was 0.25°, 0.5° or 1°, frequency was 80, 100, 150 or 250 Hz, and the damping ratio was fixed at 0.08. We compared the resulting estimates with the known injected waveforms through waveform correlation, amplitude agreement and the reduction in error of the estimated head trajectory. Discrimination between recordings with injected relative motion and the smooth-head null gave a further measure of performance. These experiments characterize behaviour within specified synthetic families; they say nothing about how often such disturbances arise with the ACT headband during actual sporting activity.

2.7 Mechanical descriptors, H1 scores and statistical analysis

To see how the decomposition affected subsequent mechanical analysis, we applied the frozen IFS V2.0 battery to each eligible recording in two forms, first to the original gyroscope waveform and then to the HDA-estimated head angular velocity obtained with θ_max = 0.25°. The paired design yields 14 mechanical descriptor coordinates and two peak angular comparators for each signal representation. From the same pair of representations we calculated five H1 scores: the four mechanical-domain scores and the overall descriptive score. The analysis manifest documents the IFS definitions, the checksums of the frozen modules and the unchanged reference derived from 299 male-football initial triggers. H1 is a distribution-relative descriptive scoring layer, not a quantity in joules and not a clinical measure. Its interpretation needs particular care here, because applying a reference derived from recorded sensor signals to HDA-corrected trajectories changes what a position in that reference distribution means.

We made the principal descriptive comparison within events, holding the event population constant and changing only the waveform representation supplied to the mechanical battery. For descriptor x, the archived computation defined absolute relative change as $100|x_{HDA} - x_{recorded}| / \max(|x_{recorded}|, 10^{-12})$, and we then calculated medians and 90th percentiles of that quantity across events. This definition reproduces the archived computation, but it cannot be read as an ordinary percentage change for an event whose recorded baseline is exactly zero. We therefore give the numbers of such events in the main tables and, for C06, a separate median calculated only among events with nonzero recorded values. H1 changes are expressed directly in score points, as HDA-estimated minus recorded score, and summarized by median and interquartile range. We recalculated the descriptive changes, population counts and input checksums independently from the retained v0.1.2 outputs. That reconciliation did not rerun the original HDA decomposition, the event classifiers or the mixed-effects models.

Earlier exploratory analyses give additional context for the descriptive comparisons, although they belong to earlier analytic stages. They include Mann-Whitney U comparisons, log-linear models adjusted for the recorded peak angular velocity, and mixed-effects models with a random intercept for sensor profile. Event-classification performance was examined by repeated stratified or profile-grouped cross-validation with random forests [21] and histogram gradient boosting [22]. We retain these results with their original model specifications and cohort definitions, documented in Supplementary Sections C and D, and do not present them as newly fitted analyses. The distinction matters most for the hockey event-context comparisons: the historical analyses used a 372/4,030 division, whereas the accepted IFS analysis uses 367/4,035. Estimates from the former definition have not been silently reassigned to the latter population.

2.8 Cumulative mechanical-exposure demonstration

We intend to extend the paired event-level comparison to repeated participation in ice hockey. The estimand is the player-match and player-season sum of C01 and C02 over exactly the same Wisehockey-

confirmed on-ice events before and after correction, so that the effect of HDA is separated from the effect of event selection, together with the paired difference between those sums, the relative difference where the recorded total is strictly positive, and the corresponding rate per minute of verified time on ice. Accumulated mechanical descriptors are not a biological injury dose, and their interpretation depends on the validity of the underlying measurements and on the completeness of event capture. Supplementary Section D.6 specifies the estimand, the coverage rules for player-matches without detected events, and the descriptive player-ranking comparisons in full. The calculation awaits the season-wide Wisehockey event classification and the player-match time-on-ice denominators, which have not been materialized in this analysis workspace.

2.9 Reproducibility and publication ethics

Reproducibility of the present numerical comparisons rests on the retained input files, software versions and analysis manifests, not on reconstruction from reported aggregate values. The archived software analyses carry version HDA 0.1.2. In HDA 0.2.0 the decomposition solver and the IFS/H1 bridge are byte-identical to that version. The release adds output columns, compares null percentiles with an amplitude-matched null, adds one artefact rule and corrects a timestamp conversion that affected only the time-window artefact and admissibility indicators. None of these changes enters the comparisons reported here, so the reported values hold unchanged for version 0.2.0. For each source export, the manifest records the HDA version, the SHA-256 fingerprint of the input file, the solver parameters, the sensor-excursion sweep, the synthetic null reference and the checksums of the frozen IFS modules. The retained descriptive-analysis script reads the event-level output tables, performs the paired calculations and leaves the original files untouched. Release of the HDA program, its tests, the synthetic examples and selected demonstrator recordings is planned with a later version of this work prepared for journal submission, with release of de-identified participant waveforms conditional on the existing permissions that govern their use. Its licensing terms will be stated with that release.

Two distinct consent and oversight arrangements covered the empirical analyses. The women's ice-hockey recordings originated in the Sustainable Careers in Elite Contact Sports (SUCCESS) study, for which the Ethics Committee of Helsinki University Hospital granted approval (HUS/5422/2024, 3 July 2024), and participants gave written informed consent. The football data came from adult volunteers during ordinary sporting activity, with written consent collected and retained by the participating clubs. This non-interventional collection involved neither clinical assessment nor interventions affecting physical integrity, and it therefore required no statutory ethics approval under the Finnish Medical Research Act (488/1999). Under the guidelines of the Finnish National Board on Research Integrity governing non-medical research with human participants, the reported protocol likewise met no criterion requiring prospective human-sciences ethical review. The analyses used pseudonymized sensor records and involved no health outcomes. We excluded data collected from minors and from the boxing test session for which prior consent had not been obtained.

Large language models from Anthropic (Claude) and OpenAI (ChatGPT) assisted iterative software prototyping, technical review, analysis planning and manuscript preparation during development. The

human authors retain responsibility for the scientific decisions, the verification of source code and numerical results, the interpretation of the evidence and the final manuscript text.

3 Results

3.1 Synthetic validation of bounded-excursion decomposition

Our choice of head-side objective came out of the synthetic experiments. A torque-rate formulation investigated first behaved mainly as a smoothing criterion: at θ_max = 0.5° it removed a median 97% of inertial demand even in the smooth synthetic null, where no sensor-relative motion had been introduced. We therefore kept the first-difference torque criterion. Under that criterion and θ_max = 0.1°, discrimination of recordings containing injected sensor-relative ringing from the smooth rigid-head null depended on the injection configuration, with areas under the receiver operating characteristic curve from 0.94 to 1.00 (Table 1). At the best-tested excursion bound, correlations between the injected and HDA-attributed relative angular-velocity waveforms ran from 0.83 to 0.91, and head-trajectory error fell by 43 to 58%. Recovery of the injected motion came at a price: as the allowed excursion grew, some genuine simulated head motion was removed along with it. In the smooth-head null, the angular-velocity norm assigned to the sensor-relative component rose from 1.8% at 0.05° to 2.9%, 5.8%, 9.6%, 15.9% and 26.8% at 0.1°, 0.25°, 0.5°, 1° and 2°. The predefined 0.25° bound must therefore be read as a pragmatic setting for the present analysis and not as an individually measured limit of attachment motion.

Table 1
Synthetic injection recovery. Historic validation results from the October manuscript; the source code and validation records retain full provenance.

Injected relative rotation	Detection AUC (ΔJ_rel at 0.1°)	Attributed/injected waveform correlation (bound)	Head-trajectory error reduction
0.25°, 100 Hz	0.94	0.83 (0.1°)	43%
0.5°, 80 Hz	0.95	0.86 (0.25°)	48%
0.5°, 150 Hz	1.00	0.89 (0.25°)	54%
0.5°, 250 Hz	1.00	0.88 (0.25°)	51%
1.0°, 150 Hz	0.98	0.91 (0.5°)	58%

3.2 Football: correction of video-classified individual recordings

We evaluated the event-level application in the 341 recordings uniquely matched to the video-review master. Every one of these initial triggers produced valid HDA and frozen-IFS outputs, so the recorded and estimated head-motion representations could be compared within the same independently labelled events. Among the 233 video-confirmed headers, changes were comparatively small for C05 angular

activity and C02 rotational energy-time, with median absolute relative changes of 2.57% and 6.55%. The corresponding changes reached 27.01% for C01 rotational co-activity, 30.69% for C03 directional load and 25.20% for C07 angular-axis path. The 108 non-header recordings showed the same contrast, with medians of 2.26% for C05 and 5.92% for C02 against 29.82% for C01, 34.06% for C03 and 25.70% for C07. Integrated angular activity thus moved modestly while the estimated sensor-relative contribution had a much larger effect on descriptors that depend on temporal and directional detail of the waveform. Table 2 gives the complete mechanical battery, the peak comparators and every H1 domain for both video classes.

Table 2

Video-confirmed football events: complete frozen IFS mechanical descriptor and H1 comparison. Event-level paired changes from recorded gyroscope to the HDA-estimated angular waveform at θ_max = 0.25°. Each of the first 16 rows reports median absolute relative change (%), calculated under the archived denominator-floor convention; the last five rows report median paired H1 change in points [25th, 75th percentiles]. The zero columns identify exact recorded-baseline zeroes, for which the ordinary percentage change is undefined. n = 233 headers and 108 non-headers.

Descriptor or H1 domain	Headers	Non-headers	Recorded zero baselines (header / non-header)
C01 rotational co-activity	27.01%	29.82%	0 / 0
C02 rotational energy-time	6.55%	5.92%	0 / 0
C03 directional load	30.69%	34.06%	1 / 1
C05 angular activity	2.57%	2.26%	0 / 0
C05 active fraction	0.00%	0.78%	0 / 0
C06 post-peak re-acceleration	39.34%	44.31%	44 / 25
C07 axis path	25.20%	25.70%	1 / 1
C07 PCA dominance	2.66%	2.26%	0 / 0
C08 energy entropy	1.96%	1.84%	0 / 0
C09 tail fraction	5.89%	4.43%	0 / 0
C10 peak count	0.00%	0.00%	81 / 45
C10 secondary ratio	0.00%	0.00%	180 / 91
C11 envelope correlation	7.55%	10.84%	0 / 0
C12 speed spectral entropy	8.95%	13.31%	0 / 0
Peak angular velocity	3.63%	7.07%	0 / 0
Peak angular acceleration	18.26%	30.54%	0 / 0
H1 domain changes, points	Median [Q1, Q3]	Median [Q1, Q3]	n
Rotational loading	-3.01 [-5.02, -1.51]	-2.84 [-4.72, -1.67]	233 / 108

For C06 specifically, the nonzero-baseline restricted medians were 46.43% (189 headers) and 57.27% (83 non-headers). C10 counts/ratios are discrete and can have a median floor-based change of zero even when a subset changes. Original source: independently recalculated HDA v0.1.2 data tables; audit script and input hashes retained.

Descriptor or H1 domain	Headers	Non-headers	Recorded zero baselines (header / non-header)
Directional mechanics	-6.02 [-10.79, -3.18]	-7.15 [-11.15, -3.26]	233 / 108
Temporal organization	-1.11 [-3.62, + 0.17]	-0.84 [-5.18, + 0.15]	233 / 108
Motion coordination	+ 0.50 [-2.84, + 5.18]	-0.25 [-5.23, + 2.26]	233 / 108
Overall H1	-2.29 [-4.66, -0.85]	-2.85 [-5.41, -0.73]	233 / 108
For C06 specifically, the nonzero-baseline restricted medians were 46.43% (189 headers) and 57.27% (83 non-headers). C10 counts/ratios are discrete and can have a median floor-based change of zero even when a subset changes. Original source: independently recalculated HDA v0.1.2 data tables; audit script and input hashes retained.			

Post-peak re-acceleration, C06, needs a separate qualification, because a substantial number of events have a recorded baseline of zero. Under the archived denominator-floor calculation, the median absolute relative change in C06 was 39.34% in headers and 44.31% in non-headers. Restricting the comparison to recordings with nonzero baseline C06 gives medians of 46.43% for 189 headers and 57.27% for 83 non-headers. The two calculations answer different questions and should not be interchanged. Absolute paired differences and an explicit description of transitions from a zero baseline are necessary complements to any percentage summary of this descriptor.

We also examined how the HDA representation related to the video-label classification analyses developed earlier, treating classification as secondary to mechanical estimation. In the archived profile-grouped cross-validation, a classifier built on 16 HDA output variables reached an ROC-AUC of 0.769. The complete 339-feature IFS V4.11 representation reached 0.826, and adding the HDA variables left it at 0.826. Within the smaller frozen IFS V2.0 battery, the 14 mechanical coordinates gave almost identical profile-grouped discrimination whether calculated from recorded or corrected angular waveforms, at 0.704 and 0.705. These values come from the historical classifier runs and were not refitted for the present revision. They demonstrate neither an improvement nor a deterioration in established header discrimination attributable to HDA, and they are no substitute for assessing the mechanical interpretation of the estimated trajectories.

Figure 2 shows four of the video-confirmed events, selected by a fixed rule from the HDA 0.2.0 output so that each video class is represented by one event with a small and one with a substantial correction. Eligible events were initial triggers with a valid solution, no saturated gyroscope sample, the first live gyroscope sample at 8 ms, an admissible head estimate, an artefact indicator level of head-like (0 to 1 points) and a recorded peak angular velocity of at least 5 rad/s, which left 154 headers and 55 non-headers. Within each class we took the events whose attributed energy share at θ_max = 0.25° lay closest to the class 10th and 90th percentiles. All four selected events came from the male session.

With small corrections (E_frac 0.5% and 0.6%), the head estimate follows the recorded trace closely and peak angular velocity changes by at most 0.7 rad/s. With substantial corrections (E_frac 6.3% and 7.1%), the head estimate loses part of the oscillatory structure that follows contact, and peak angular velocity falls from 5.9 to 4.8 rad/s in the header and from 9.1 to 7.4 rad/s in the non-header. Panel A also shows a step in the head estimate at the end of a long contact interval, a property of the method described in Supplementary Section A.6.

3.3 Ice hockey: whole-season effects on mechanical descriptors

The larger empirical application covered all 17,607 Auroraliiga recordings with usable gyroscope input. HDA v0.1.2 converged for every one of them, and we reconciled the complete set of frozen-IFS outputs independently. The earlier hockey IFS exports proved byte-identical to the corresponding v0.1.2 files, which supports the reproducibility of the archived descriptor comparisons without implying that the HDA decomposition was rerun independently. At θ_max = 0.1°, the attributed sensor-relative component had a median effective frequency of 89.90 Hz, with an interquartile range from 75.03 to 106.72 Hz. That frequency does not measure mounting resonance directly: the optimisation criterion preferentially assigns high-frequency motion to the relative component, and the resulting effective frequency also depends on the excursion envelope the model allows.

As in football, the size of the correction varied across mechanical descriptors. Over the entire hockey cohort, median absolute relative changes stayed modest for the integrated quantities C05 angular activity (1.69%) and C02 rotational energy-time (4.51%), and were substantially larger for C01 rotational co-activity (25.91%), C03 directional load (25.90%) and C07 axis path (21.13%). Two further descriptors, C11 envelope correlation and C12 angular-speed spectral entropy, changed by medians of 8.13% and 9.13%. The peak comparators showed the same divide: peak angular velocity changed by a median 4.43% and peak angular acceleration by 27.95%. Temporal derivatives and directional organization are thus affected by the decomposition differently from the more integrated angular measures. Table 3 reports all 16 mechanical coordinates and comparators, not only those singled out here for interpretation.

Table 3

Whole-season women's ice hockey: complete frozen IFS mechanical descriptor and H1 comparison. The first 16 rows report the median absolute relative change (%) and 90th percentile (%) under the archived denominator-floor convention across 17,607 gyroscope-analyzable recordings. Because relative change is undefined when a recorded baseline equals zero, the penultimate column gives the number of zero-baseline events and the last column gives the nonzero-baseline-only median. H1 rows report paired change in score points with quartiles; n for motion coordination is 17,606, otherwise 17,607.

Descriptor or H1 domain	Floor-based median	90th percentile	Recorded baseline = 0 (n)	Nonzero-baseline median
C01 rotational co-activity	25.91%	76.11%	1	25.91%
C02 rotational energy-time	4.51%	25.59%	0	4.51%
C03 directional load	25.90%	83.61%	904	27.90%
C05 angular activity	1.69%	11.10%	0	1.69%
C05 active fraction	0.00%	17.86%	0	0.00%
C06 post-peak re-acceleration	41.22%	100.00%	3231	54.82%
C07 axis path	21.13%	74.31%	914	23.07%
C07 PCA dominance	1.49%	9.54%	0	1.49%
C08 energy entropy	1.50%	14.05%	0	1.50%
C09 tail fraction	3.48%	21.60%	0	3.48%
C10 peak count	0.00%	100.00%	7805	0.00%
C10 secondary ratio	0.00%	100.00%	14600	100.00%
C11 envelope correlation	8.13%	91.59%	0	8.13%
C12 speed spectral entropy	9.13%	41.66%	0	9.13%
Peak angular velocity	4.43%	27.79%	0	4.43%
Peak angular acceleration	27.95%	81.73%	1	27.95%

In C06, the 3,231 zero-baseline recordings comprise 2,936 zero-to-zero and 295 zero-to-positive transitions. The nonzero-only C06 median, 54.82%, is the figure to use when describing conventional relative percentage change. Values in the floor-based column are retained to reproduce the historical analysis and not to interpret zero-baseline changes as percentages. The C10 secondary ratio illustrates the same point from the opposite direction: 14,600 of the 17,607 recordings have a recorded baseline of zero, which places the floor-based median at 0.00%, while the median among the 3,007 recordings with a nonzero baseline is 100.00%. The two columns describe different subsets of events and are not in conflict.

Descriptor or H1 domain	Floor-based median	90th percentile	Recorded baseline = 0 (n)	Nonzero-baseline median
H1 score changes, points	Median	Q1	Q3	n
Rotational loading	-2.51	-5.18	-0.67	17607
Directional mechanics	-4.68	-10.45	-1.92	17607
Temporal organization	-1.14	-5.07	0.00	17607
Motion coordination	-0.84	-5.18	1.51	17606
Overall H1	-2.73	-5.87	-0.91	17607

In C06, the 3,231 zero-baseline recordings comprise 2,936 zero-to-zero and 295 zero-to-positive transitions. The nonzero-only C06 median, 54.82%, is the figure to use when describing conventional relative percentage change. Values in the floor-based column are retained to reproduce the historical analysis and not to interpret zero-baseline changes as percentages. The C10 secondary ratio illustrates the same point from the opposite direction: 14,600 of the 17,607 recordings have a recorded baseline of zero, which places the floor-based median at 0.00%, while the median among the 3,007 recordings with a nonzero baseline is 100.00%. The two columns describe different subsets of events and are not in conflict.

Exact zero baselines again bear materially on the interpretation of C06. Its recorded value was zero in 3,231 of the 17,607 hockey events, 18.4% of the cohort. After HDA, 2,936 of those events remained at zero and 295 acquired a positive value. Including all events under the archived denominator-floor convention of 10^{-12} gives a median absolute relative change of 41.22%; among the 14,376 events with a nonzero recorded C06 the conventional median is 54.82%. The distinction is definitional and does not indicate disagreement between versions of the output files. Other coordinates, in particular the discrete peak-count and secondary-ratio measures, also contain zero baselines, and we retain their floor-based summaries for reproducibility without reading them as conventional percentage changes.

We evaluated changes in the H1 scoring layer separately from changes in the mechanical descriptors, because H1 values describe position relative to a fixed reference distribution. The overall H1 score fell by a median 2.73 points, with an interquartile range from − 5.87 to − 0.91. Directional mechanics showed the largest median shift among the four domains, at − 4.68 points. Recorded and HDA-estimated overall H1 stayed closely associated across events, with a Spearman rank correlation of 0.9666, although 30.60% of individual events differed by more than five score points in absolute value. None of these paired shifts may be read as a change in physical energy; they are changes on a reference-relative descriptive scale. Table 3 carries the complete domain results together with the corresponding sample sizes.

The archived analyses of hockey event context asked whether attributed sensor-relative motion differed between recordings made during active play and recordings made outside play. After adjustment for recorded motion magnitude they reported a larger attributed component in on-ice events, with the

associations attenuated in models that included a random intercept for sensor profile. These findings must be read with their original population definitions. The historical full-context models used 372 on-ice and 4,030 off-ice records, whereas the subsequently frozen IFS cohort definition holds 367 and 4,035. Supplementary Section D retains the model results and their provenance. Because the models were not refitted under the later classification, we do not describe them as newly estimated effects for the complete season.

3.4 Ice hockey: cumulative mechanical exposure during verified on-ice participation

This analysis is in preparation, and the present version reports no cumulative result. The longitudinal comparison will carry the corrected-versus-recorded evaluation from single events to verified on-ice participation, reporting recorded and HDA-estimated cumulative C01 and C02 over identical Wisehockey-confirmed event sets for each eligible player-match and for season totals, together with mechanical-exposure rates per minute of verified time on ice and descriptive comparisons of player ordering. Supplementary Section D.6 specifies that design, including the counts of eligible on-ice events, players, matches and zero-event player-matches that its interpretation will require. No ordering produced by it is a clinical risk classification.

4 Discussion

4.1 Principal findings and interpretation

The central methodological contribution of HDA is to make the distinction between head motion and sensor motion explicit in the analysis of wearable gyroscope recordings. The method represents the measurement as an estimated head trajectory together with a sensor-relative component that satisfies a bounded-orientation constraint, in place of treating measured angular velocity as an unqualified description of skull movement. It obtains the decomposition by minimizing head-side inertial demand outside the specified contact interval while accounting for gyroscope quantisation. What results is a reproducible conditional estimate whose assumptions can be varied and examined, not an unconstrained filtering operation. The synthetic experiments show that HDA recovers injected relative rotation under the tested conditions, and they also show how the estimate shifts when increasingly large excursions are allowed. The empirical recordings add a complementary perspective. Video verification allows the correction of identifiable football events to be studied, and the much larger hockey cohort establishes how differences between recorded and estimated head motion distribute across repeated sporting recordings. Together these findings show that the response to HDA correction is not uniform across descriptors: its size tracks the mathematical properties of the quantity being calculated.

Characterizing HDA chiefly as a method that reduces the magnitude of all recorded head motion would misrepresent it. Integrated angular-activity measures were comparatively stable in both empirical settings, while several measures involving angular acceleration or the direction and temporal

organization of movement changed materially. Mechanically this follows from the fact that a bounded change in relative orientation can produce larger changes in its time derivatives, though the empirical comparisons remain conditional on the selected model and attachment bound. The purpose of event classification raises a related point. Discriminating headers from non-headers successfully does not establish that the underlying waveform is an accurate estimate of head motion. HDA-derived attributes carried some discriminatory value in the football analysis, yet adding them to the much larger existing IFS feature representation did not improve profile-grouped classification. The principal contribution of HDA is accordingly a more explicit and testable mechanical interpretation of sensor-derived kinematics, and not a general claim of better event classification.

4.2 Physical interpretation of sensor-relative motion

Interpretation of the inferred relative component turns on the physical interface between the ACT sensor and the head. In these recordings an elastic headband compressed a small sensor against the mastoid. Its coupling cannot be assumed identical to that of a helmet shell or an instrumented mouthguard, even though work with those systems establishes that relative movement at the measurement interface can alter recorded kinematics [3–8]. Displacement amplitudes and characteristic frequencies reported for other attachments cannot simply be carried over to the ACT model. HDA asks instead how much post-contact inertial demand can be avoided while the relative sensor orientation varies within a specified envelope. The sensor-relative waveform that emerges is an inference under mechanical constraints and not an independently measured displacement of skin or attachment. The same caution applies to its effective frequency. Because the optimization preferentially allocates certain rapid variations to the sensor-relative component, a high effective frequency cannot by itself identify a natural vibration frequency of the headband or the sensor mounting.

The earlier labelled hockey analysis shows why sensor-relative movement and handling artefact should not be treated as synonyms. Within that analysis, on-ice recordings carried a larger attributed relative component than off-ice recordings even though their mean rotational magnitudes were smaller. Legitimate contact during play can plausibly excite the sensor attachment, so a relative contribution need not mean that the event was unrelated to head movement. Handling an unworn sensor may in turn generate a signal mechanically unlike the constrained movement of a sensor pressed against the mastoid, though the decomposition alone cannot settle that. The origin of a recording and the reliability of a particular kinematic quantity remain separate questions. A quality-control system intended for sporting exposure research must preserve that separation instead of equating every estimated relative movement with an invalid event.

4.3 Implications for IFS and cumulative mechanical exposure

Interpreting the descriptor results depends on keeping HDA and the frozen IFS battery apart. HDA changes the angular-velocity trajectory supplied to the calculation while the mathematical definitions of the IFS coordinates stay fixed. Each recorded-versus-corrected pair therefore measures the sensitivity of

an unchanged descriptor to the inferred sensor-relative contribution. In the football and hockey analyses alike, C05 and C02 were relatively stable while C01, C03, C06 and C07 were more sensitive. Different mechanical representations of the same recording can thus respond quite differently to an estimation procedure that acts on waveform structure. Stability is not biological validity. A descriptor that changes little under HDA has not thereby been shown to predict injury, just as one that changes substantially is not necessarily uninformative. The comparison identifies which properties of the signal depend more strongly on the decomposition and so call for more careful interpretation in subsequent exposure analyses.

Sports monitoring accumulates information across many recordings instead of relying on individual impacts alone, which gives a further reason to examine what HDA implies. Summation suits mechanically additive quantities as long as their event-level meaning and units are preserved, but an accumulated value inherits any uncertainty about the origin of the events that feed it. In ice hockey an acceleration threshold may be crossed while a sensor is being handled or while its wearer is off the ice, and counting such records as on-ice mechanical exposure would mix sporting participation with unrelated activity. The existing Wisehockey classification offers an independent basis for limiting accumulation to verified on-ice participation [19], and recorded time on ice provides the denominator needed to compare athletes with unequal participation. Applying recorded and HDA-estimated C01 and C02 to the same eligible events then isolates the difference attributable to head-motion estimation from the difference caused by selecting a different sample. Should correction change the ordering of players by cumulative total, that would indicate measurement-dependent reordering of exposure and not a difference in concussion risk.

4.4 Limitations

The principal limitation of HDA is that the inferred division between head motion and sensor-relative motion is conditional on a model and is not identified independently from the single-sensor record. We did not measure the relative excursion envelope for each athlete, and we did not compare the estimated head trajectory with direct bone-coupled measurements. The objective that favours the head-side trajectory represents inertial demand outside the contact interval; it does not yet amount to a full head-neck model with independently measured stiffness, damping, muscular activation or physiologically calibrated torque bounds. Rapid genuine head movement may in consequence be assigned in part to the sensor when its temporal structure is also compatible with a bounded relative excursion. Synthetic null experiments expose this tradeoff under controlled assumptions, but their estimates of false attribution hold only for the simulated head-motion families and cannot establish an equivalent error rate for all athletic events or attachment conditions.

The acquisition process imposes further constraints that no decomposition can remove. Gyroscope sampling starts after accelerometer acquisition, and the historical flattened inputs additionally blank the first gyroscope samples by convention. Some of the earliest angular response may thus be missing, and the contact interval used to delimit externally forced motion may already have begun before the first live angular sample. When an angular channel saturates, HDA flags the affected measurements and omits

the corresponding rows from its demand calculation; it does not reconstruct the information lost to saturation. The linear-acceleration channels are not decomposed either, so descriptors combining linear and angular information use the original linear measurements together with the HDA-estimated angular trajectory, a distinction that must be kept in their interpretation. Event acquisition finally depends on the sensor's linear-acceleration trigger threshold, which shapes which impacts enter a dataset at all [24, 25]. Since the analysis begins with already triggered records, it cannot recover head motions that failed to trigger acquisition in the first place.

The observational datasets carry limitations independent of the mechanical model. One reviewer assigned the football labels from video, and the male and female recordings each came from a single training session. Sex is therefore confounded with session-specific heading technique, acquisition conditions and sensor fitting, which prevents any separate interpretation of apparent sex differences in these data. Events from the same athletes share participant and attachment characteristics, so repeated observations cannot be assumed independent. For the hockey analyses we retain the historical classification and mixed-effects results with their original definitions and software provenance; they have not been refitted after later revisions to event-context classification. The whole-cohort HDA/IFS descriptive comparisons have been reconciled independently, but the separate aggregation by player and match remains unfinished. We therefore make no claim that a season-wide cumulative-load effect has already been observed. Reaching such a conclusion will require the independently classified on-ice events and the complete exposure denominators to be linked and the paired totals to be calculated.

These qualifications also delimit any clinical reading of the findings. Neither the original sensor waveform nor an HDA-derived mechanical descriptor measures intracranial pressure, tissue strain or brain injury directly, and we analysed no clinical outcomes. HDA should accordingly be evaluated and described as a method for estimating mechanical head motion under stated assumptions, not as a diagnostic instrument or a measure of injury severity.

4.5 Future methodological development

Several extensions follow from the present mechanical formulation. A calibrated model of head-neck dynamics could replace or supplement the current inertial-demand objective, carrying measured limits on passive mechanical response and on active muscular contributions including stiffness, damping and torque generation [15–18, 26]. Such a model would distinguish mechanically plausible rapid head movement from motion more reasonably assigned to the attachment. Information about the mounting properties of an individual athlete or sensor profile, estimated at session level, could in parallel give more specific bounds on relative excursion than the common set of radii used here. A further extension would bring the linear-acceleration channels into the same estimation and improve the definition of the contact interval, addressing uncertainty in translational movement and in the earliest part of the recorded event. Each of these developments would have to be assessed against the measurement interface: assumptions formulated for an ACT sensor pressed against the mastoid should not be transferred to helmet or mouthguard systems without independent coupling validation.

4.6 Conclusions

A mastoid-mounted inertial sensor records its own movement, which may include motion relative to the head. HDA represents that distinction explicitly by decomposing the angular-velocity waveform under separate head-side and sensor-side constraints. In synthetic tests the method recovered known injected relative motion within the conditions examined, and the paired comparisons in video-verified football events and in the large hockey cohort showed how differently mechanical descriptors respond to the estimated relative component. HDA is best understood as a conditional head-motion estimator with an accompanying sensitivity-analysis layer, not as a direct measurement of skull movement. Applied to repeated events, it also gives a defined basis for investigating cumulative mechanical exposure, provided that on-ice events are independently identified, that recording coverage is established and that suitable monitoring denominators are available.

Declarations

Data availability

The browser version of the HDA viewer, available at http://impactfeaturespace.com/hda-viewer/, shows a random sample of the analysed events: 25% of each football session and 10% of the ice-hockey events of four players over twelve match days, with randomly coded athletes and fictitious dates and clock times. Athlete-linked event-level datasets and comprehensive match-linked data cannot be made public, because of consent, privacy and source-data restrictions. Requests for controlled access may be directed to the corresponding author and will be reviewed subject to the governing ethics, participant consent and data-use restrictions.

Code availability

The HDA program (version 0.2.0) is not released with this version of the manuscript. The analyses reported here were run with version 0.1.2; because the decomposition and the IFS/H1 bridge are identical in 0.2.0 (Section 2.9), the reported values apply to version 0.2.0. Section 2 and Supplementary Section A give the measurement model, the discretisation, the objective, the constraints and the solver settings. A self-contained browser version of the HDA viewer, which displays precomputed HDA 0.2.0 output and does not contain the method itself, can be opened without installation at http://impactfeaturespace.com/hda-viewer/. Release of the program is planned with a later version of this work prepared for journal submission. The separately restricted IFS code is not included.

Author contributions

JL conceived and developed the HDA method and software, performed the data analysis, and drafted the manuscript. KP contributed to data collection, study design, interpretation, and critical revision. MV contributed to data collection, study design, interpretation, and critical revision. LH contributed to study design, neurological and neuropsychological interpretation, critical revision, supervision, and funding. TM

contributed to data collection, study design, interpretation, and critical revision. JK contributed to data collection, study design, interpretation, and critical revision. All authors read and approved the manuscript.

Funding

This work received no specific funding.

Competing interests

J.L. is named as an inventor on a pending patent application filed with the Finnish Patent and Registration Office concerning methods for extracting and representing waveform-derived features from wearable head-impact sensor data, including aspects of the Impact Feature Space methodology used in this manuscript. The patent application was filed before submission of the manuscript. No licensing income or commercial revenue has been received. The other authors declare no competing interests.

References

1. O'Connor KL, Rowson S, Duma SM, Broglio SP (2017) Head-impact-measurement devices: A systematic review. J Athl Train 52(3):206–227. https://doi.org/10.4085/1062-6050.52.2.05X
2. Le Flao E, Siegmund GP, Borotkanics R (2022) Head impact research using inertial sensors in sport: A systematic review of methods, demographics, and factors contributing to exposure. Sports Med 52(3):481–504. https://doi.org/10.1007/s40279-021-01574-y
3. Wu LC, Nangia V, Bui K, Hammoor B, Kurt M, Hernandez F, Kuo C, Camarillo DB (2016) In vivo evaluation of wearable head impact sensors. Ann Biomed Eng 44(4):1234–1245. https://doi.org/10.1007/s10439-015-1423-3
4. Joodaki H, Bailey A, Lessley D, Funk J, Sherwood C, Crandall J (2019) Relative motion between the helmet and the head in football impact test. J Biomech Eng 141(8):081006. https://doi.org/10.1115/1.4043038
5. Sciacca D, Ionescu A (2025) Helmet-head decoupling in ice hockey impacts: An in-lab exploratory study using autoregressive modeling. Ann Biomed Eng 53(11):3141–3155. https://doi.org/10.1007/s10439-025-03848-2
6. Luke D, Kenny R, Bondi D, Clansey A, Wu LC (2024) On-field instrumented mouthguard coupling. J Biomech 162:111889. https://doi.org/10.1016/j.jbiomech.2023.111889
7. Clansey AC, Bondi D, Kenny R, Luke D, Masood Z, Gao Y, Elez M, Ji S, Rauscher A, van Donkelaar P, Wu LC (2024) On-field head acceleration exposure measurements using instrumented mouthguards: Multi-stage screening to optimize data quality. Ann Biomed Eng 52(10):2666–2677. https://doi.org/10.1007/s10439-024-03592-z

8. Jones B, Tooby J, Weaving D, Till K, Owen C, Begonia M, Stokes KA, Rowson S, Phillips G, Hendricks S, Falvey ÉC, Al-Dawoud M, Tierney G (2022) Ready for impact? A validity and feasibility study of instrumented mouthguards (iMGs). Br J Sports Med 56(20):1171–1179. https://doi.org/10.1136/bjsports-2022-105523
9. Wu LC, Laksari K, Kuo C, Luck JF, Kleiven S, Dale' Bass CR, Camarillo DB (2016) Bandwidth and sample rate requirements for wearable head impact sensors. J Biomech 49(13):2918–2924. https://doi.org/10.1016/j.jbiomech.2016.07.004
10. Gabler L, Patton D, Begonia M, Daniel R, Rezaei A, Huber C, Siegmund G, Rooks T, Wu LC (2022) Consensus Head Acceleration Measurement Practices (CHAMP): Laboratory validation of wearable head kinematic devices. Ann Biomed Eng 50(11):1356–1371. https://doi.org/10.1007/s10439-022-03066-0
11. Kuo C, Patton D, Rooks T, Tierney G, McIntosh A, Lynall R, Esquivel A, Daniel R, Kaminski T, Mihalik J, Dau N, Urban J (2022) On-field deployment and validation for wearable devices. Ann Biomed Eng 50(11):1372–1388. https://doi.org/10.1007/s10439-022-03001-3
12. Zhan X, Li Y, Liu Y, Cecchi NJ, Raymond SJ, Zhou Z, Alizadeh HV, Ruan J, Barbat S, Tiernan S, Gevaert O, Zeineh MM, Grant GA, Camarillo DB (2023) Machine-learning-based head impact subtyping based on spectral densities of head kinematics. J Sport Health Sci 12(5):619–629. https://doi.org/10.1016/j.jshs.2023.03.003
13. Launes J, Peltonen K, Vartiainen M, Hokkanen L Impact Feature Space for Wearable Sensor Head-Motion Analysis in Sport. Accepted manuscript; final journal citation pending
14. Yoganandan N, Pintar FA, Zhang J, Baisden JL (2009) Physical properties of the human head: Mass, center of gravity and moment of inertia. J Biomech 42(9):1177–1192. https://doi.org/10.1016/j.jbiomech.2009.03.029
15. Tangorra JL, Jones LA, Hunter IW (2003) Dynamics of the human head-neck system in the horizontal plane: Joint properties with respect to a static torque. Ann Biomed Eng 31(5):606–620. https://doi.org/10.1114/1.1566772
16. Le Flao E, Brughelli M, Hume PA, King D (2018) Assessing head/neck dynamic response to head perturbation: A systematic review. Sports Med 48:2641–2658. https://doi.org/10.1007/s40279-018-0984-3
17. Vasavada AN, Li S, Delp SL (1998) Influence of muscle morphometry and moment arms on the moment-generating capacity of human neck muscles. Spine 23(4):412–422
18. Eckner JT, Oh YK, Joshi MS, Richardson JK, Ashton-Miller JA (2014) Effect of neck muscle strength and anticipatory cervical muscle activation on the kinematic response of the head to impulsive loads. Am J Sports Med 42(3):566–576. https://doi.org/10.1177/0363546513517869
19. Wisehockey Ltd (2025) Wisehockey real-time ice hockey analytics platform. https://wisesport.com/hockey(accessed October 2025)
20. Goulart PJ, Chen Y (2024) Clarabel: An interior-point solver for conic programs with quadratic objectives. arXiv:2405.12762. https://arxiv.org/abs/2405.12762

21. Breiman L (2001) Random forests. Mach Learn 45(1):5–32. https://doi.org/10.1023/A:1010933404324
22. Pedregosa F, Varoquaux G, Gramfort A, Michel V, Thirion B, Grisel O et al (2011) Scikit-learn: Machine learning in Python. J Mach Learn Res 12:2825–2830
23. Wu LC, Kuo C, Loza J, Kurt M, Laksari K, Yanez LZ, Senif D, Anderson SC, Miller LE, Urban JE, Stitzel JD, Camarillo DB (2018) Detection of American football head impacts using biomechanical features and support vector machine classification. Sci Rep 8:855. https://doi.org/10.1038/s41598-017-17864-3
24. Wang T, Kenny R, Wu LC (2021) Head impact sensor triggering bias introduced by linear acceleration thresholding. Ann Biomed Eng 49(12):3189–3199. https://doi.org/10.1007/s10439-021-02868-y
25. King D, Hume P, Gissane C, Brughelli M, Clark T (2016) The influence of head impact threshold for reporting data in contact and collision sports: Systematic review and original data analysis. Sports Med 46(2):151–169. https://doi.org/10.1007/s40279-015-0423-7
26. Cournoyer J, Koncan D, Gilchrist MD, Hoshizaki TB (2021) The influence of neck stiffness on head kinematics and maximum principal strain associated with youth American football collisions. J Appl Biomech 37(3):288–295. https://doi.org/10.1123/jab.2020-0070
27. Camarillo DB, Shull PB, Mattson J, Shultz R, Garza D (2013) An instrumented mouthguard for measuring linear and angular head impact kinematics in American football. Ann Biomed Eng 41(9):1939–1949. https://doi.org/10.1007/s10439-013-0801-y

Figures

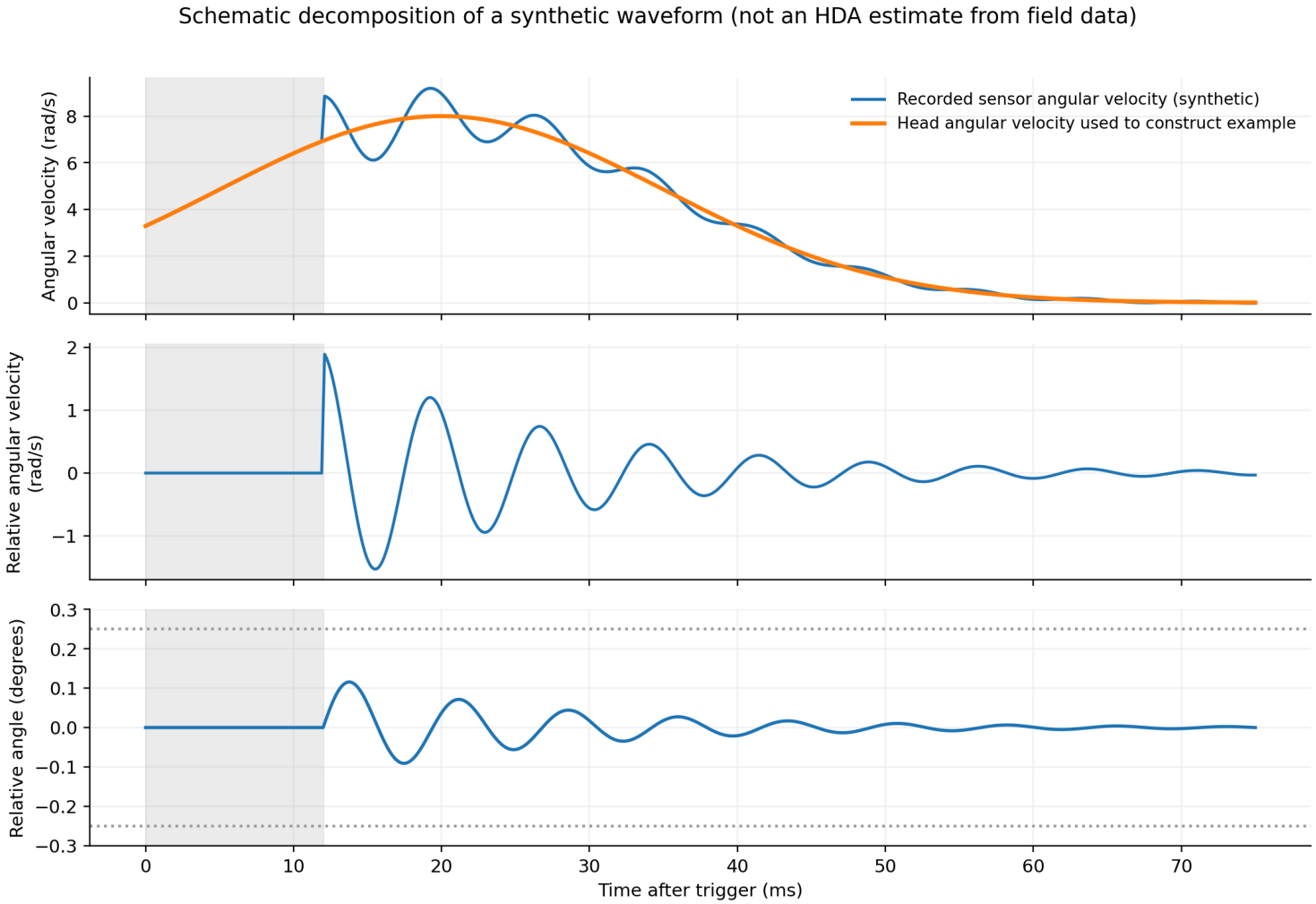


Figure 1

Figure 1. Schematic HDA decomposition of a synthetic waveform; the curves are constructed for illustration and are not an HDA estimate from field data. Top: recorded sensor angular velocity and the head angular velocity used to construct the example. Middle: sensor-relative angular velocity, a damped oscillation that begins at the end of the contact interval. Bottom: the corresponding relative angle, which stays within an excursion bound of ±0.25° (dotted lines). Grey shading marks the contact interval.

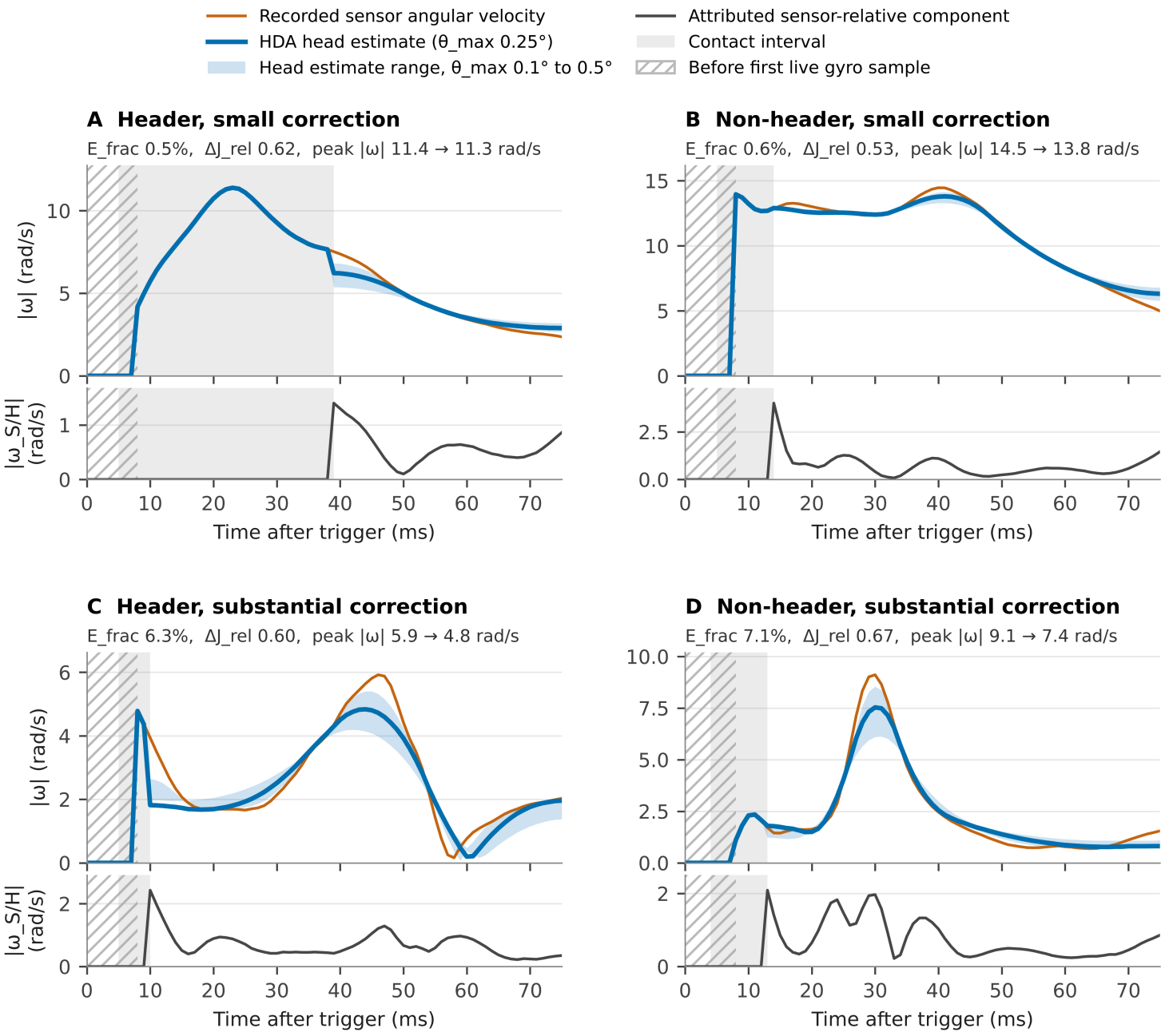


Figure 2

Figure 2. Four video-verified football events: a header and a non-header, each with a small and a substantial HDA correction (HDA 0.2.0). Upper panels: magnitude of the recorded sensor angular velocity (orange) and of the HDA head estimate at θ_max = 0.25° (blue), with the range of the head estimate between θ_max = 0.1° and 0.5° (light blue). Lower panels: magnitude of the attributed sensor-relative angular velocity. Grey shading marks the accelerometer-defined contact interval; hatching marks samples before the first live gyroscope sample. E_frac, share of angular-velocity energy attributed to sensor-relative motion; ΔJ_rel, relative reduction of post-contact inertial demand at θ_max = 0.25°. Events were selected by the rule given in Section 3.2 and Supplementary Section C.5. Athlete identifiers and timestamps are omitted.

Supplementary Files

This is a list of supplementary files associated with this preprint. Click to download.

- HDAPreprintSupplement20261116.docx